ADVANCED MATERIALS
www.advmat.de

Versatile Assembly of Metal–Phenolic Network Foams Enabled by Tannin–Cellulose Nanofibers

Bruno D. Mattos, Ya Zhu, Blaise L. Tardy, Marco Beaumont, Ana Carolina R. Ribeiro, André L. Missio, Caio G. Otoni, and Orlando J. Rojas**

Metal–phenolic network (MPN) foams are prepared using colloidal suspensions of tannin-containing cellulose nanofibers (CNFs) that are ice-templated and thawed in ethanolic media in the presence of metal nitrates. The MPN facilitates the formation of solid foams by air drying, given the strength and self-supporting nature of the obtained tannin–cellulose nanohybrid structures. The porous characteristics and (dry and wet) compression strength of the foams are rationalized by the development of secondary, cohesive metal-phenolic layers combined with a hydrogen bonding network involving the CNF. The shrinkage of the MPN foams is as low as 6% for samples prepared with 2.5–10% tannic acid (or condensed tannin at 2.5%) with respect to CNF content. The strength of the MPN foams reaches a maximum at 10% tannic acid (using $Fe^{(III)}$ ions), equivalent to a compressive strength 70% higher than that produced with tannin-free CNF foams. Overall, a straightforward framework is introduced to synthesize MPN foams whose physical and mechanical properties are tailored by the presence of tannins as well as the metal ion species that enable the metal–phenolic networking. Depending on the metal ion, the foams are amenable to modification according to the desired application.

1. Introduction

Plant-based nanomaterials and biobased polymers along with their rich set of colloidal interactions are seen as key enablers of the materials of the future bioeconomy.[1] Cellulose nanofibers (CNFs) have been used to prepare high-performance materials ranging from filaments[2] and films[3] to porous aerogels and foams.[4,5] Among the latter, cellulosic foams represent green options with potential for nontoxic thermal insulation,[6] catalytic environmental remediation,[7,8] and lightweight materials,[5] among others. Although cellulose provides robust porous scaffolds, its intrinsic chemical inertness restricts applications unless it is modified with entities holding specific functionalities (e.g., magnetism, conductivity). On that note, CNFs have been chemically modified,[9,10] composited with polymers[11,12] or nanomaterials,[6] used as a template for the growth of functional nanoparticles,[13] and more recently coassembled with metal–organic frameworks (MOFs).[14] Such efforts have enhanced their processing and uses;[1] however, most of the classical challenges related to generic nanohybridization also apply to cellulosic materials, a subject that remains poorly developed in the case of CNF.

In cellulose constructs, cellulose–cellulose interactions are superior to other noncovalent interactions. Therefore, modifying cellulose or adding a secondary phase typically reduces the structural cohesion. Furthermore, incorporating a functionality within a nanocellulose network often leads to uneven distribution, aggregation, and phase separation. Meanwhile,

B. D. Mattos, Y. Zhu, O. J. Rojas
Department of Bioproducts and Biosystems
School of Chemical Engineering
Aalto University
Vuorimiehentie 1, FI-00076 Espoo, Finland
E-mail: bruno.mattos@aalto.fi

B. D. Mattos, A. C. R. Ribeiro, A. L. Missio
Technological Development Center
Materials Science and Engineering (PPGCEM)
Federal University of Pelotas (UFPel)
Gomes Carneiro 1, Pelotas, RS 96010-610, Brazil

The ORCID identification number(s) for the author(s) of this article can be found under https://doi.org/10.1002/adma.202209685.

DOI: 10.1002/adma.202209685

B. L. Tardy
Department of Chemical Engineering
Research and Innovation Center on CO2 and Hydrogen
Center for Membrane and Advanced Water Technology
Khalifa University of Science and Technology
P.O. Box 127788, Abu Dhabi, United Arab Emirates

M. Beaumont
Department of Chemistry
Institute of Chemistry of Renewable Resources
University of Natural Resources and Life Sciences
Konrad-Lorenz-Str. 24, 3430 Tulln, Austria

C. G. Otoni
Department of Materials Engineering (DEMa)
Federal University of São Carlos (UFSCar)
Rod. Washington Luís km 235, São Carlos, SP 13565-905, Brazil

O. J. Rojas
Bioproducts Institute
Department of Chemical and Biological Engineering
Department of Chemistry and Department of Wood Science
University of British Columbia
Vancouver, British Columbia V6T 1Z4, Canada
E-mail: orlando.rojas@ubc.ca

controlled bottom-up hybridization, for instance, by in situ nanoparticle (NP) growth, leads to a better trade-off between function and strength. Nevertheless, NPs in the range of dozens of nanometers, like those grown in situ within nanocellulose networks,[13,15] proportionally offer less active sites compared to single ions. In this sense, MOF templated by nanocelluloses has been proposed to endow functionalities at the nanoscale by the effect of the corresponding metal-organic system, while largely preserving other properties.[16] Unfortunately, MOF coassembly with nanocelluloses is currently limited to a few coordination centers and ligand pairs, such as zeolotic imidazole framework (ZIF), Universitet i Oslo (UiO), and Matériaux de I'Institut Lavoisier (MIL) series.[14,17,18]

Metal–phenolic networks (MPNs) are a class of amorphous metal–organic coordination systems that exploits the ability of plant-based polyphenols to chelate metal cations for the assembly of a wide range of structures holding a much broader spectrum of metal-centered functionalities. For example, nearly 20 multivalent metal ions can be combined with plant polyphenols, as shown in the preparation of capsules,[19–21] hydrogels,[22,23] films,[24] coatings,[25] and modular supramaterials.[26] Moreover, MPNs are typically assembled in aqueous media, which facilitates coassembly with solvent-sensitive or water-holding biopolymers, such as proteins,[27] starch,[28] and cellulose.[24,29] Beyond tannic acid, typically used in MPNs, plant polyphenols include low- and high-molecular-weight tannins, either hydrolyzed or condensed, which are extracted mostly from the bark of plants using aqueous or organosolv processes.[30] Such molecules display remarkable adhesion to virtually any surface,[26] engage in multiple secondary interactions, and have a high affinity with cellulose,[31,32] which can be speculated to result from their biosynthetic pathways in plants.

Tannins and cellulose nanomaterials have been combined into lightweight porous materials with remarkable strength and insulating properties.[33,34] However, an area that still remains challenging is that related to the processing of nanocellulose suspensions in the presence of tannins and multivalent metal cations (MPN precursors), for instance, to form low density MPN foams with a homogeneous distribution of the metallic centers. Although MPNs have been assembled onto dense nanocellulose films,[24] this is more difficult in porous nanocellulose constructs given that such loose supramolecular architectures are a more delicate material to postprocess, especially in the presence of water. Furthermore, strong gels are formed between CNF and MPN precursors. The coupling of CNF-entangled network with the MPN assembly hinders the diffusion of ions and their even distribution, also leading to strong short-range interactions that collapse the network when drying-induced capillary forces take place. To address these challenges, we propose a facile method to synthesize robust MPN foams by a modified freeze–thawing–drying (FTD) of tannin-containing CNF, leading to a truly homogeneous lightweight MPN–CNF foam (**Figure 1**a–e). Whereas a classical FTD method typically uses neat ethanol for thawing,[35] we incorporated metal nitrates in the ethanolic thawing medium, enabling MPN formation in situ. Such process occurs during the thawing of the frozen structure in the presence of phenolic ligands adsorbed on the nanofibers (Figure 1b) together with solvent exchange, from H_2O to EtOH (Figure 1c). The formation of a cohesive MPN coating onto the ice-templated CNF yields a much stronger foam when compared to pure CNF foams, especially in wet conditions. This allows the wet structure to be air-dried with minimal shrinkage (Figure 1d). Such characteristics have traditionally been achieved by partial dissolution and regeneration

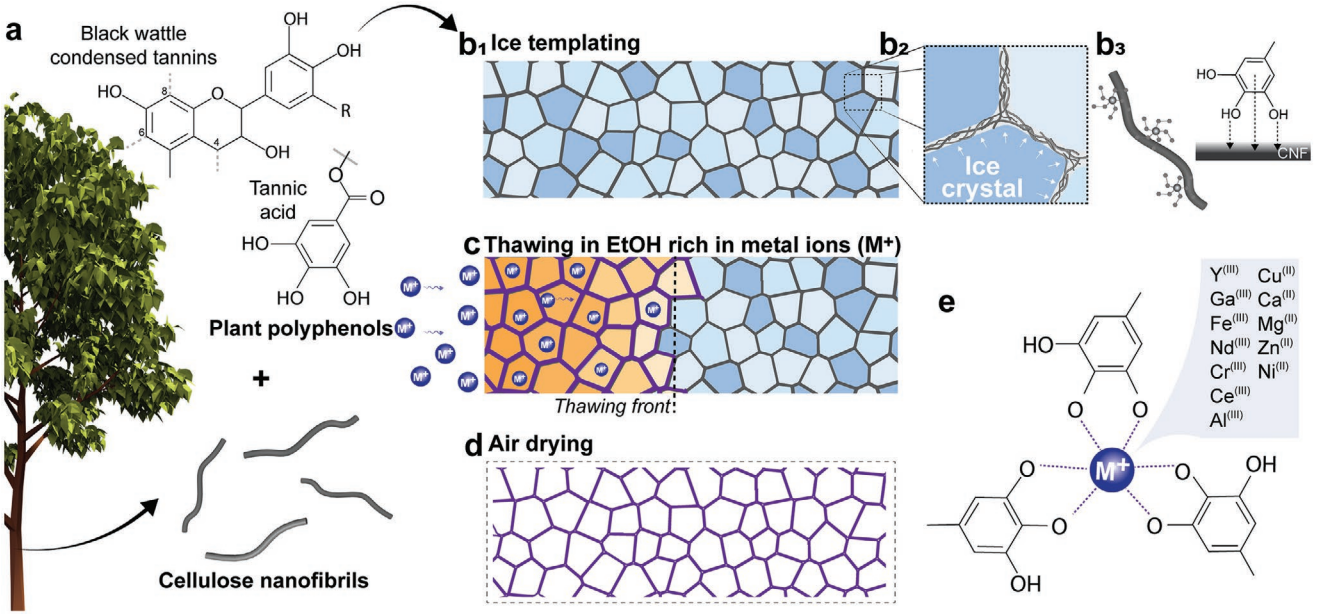

Figure 1. Renewable, plant-based materials are used to prepare strong and functional lightweight porous materials. a) Cellulose nanofibers (CNFs) are combined with either tannic acid or condensed tannins via cogrinding. b_1) The tannin–CNF is frozen and used in the formation of b_2) porous networks with cell walls that incorporate b_3) CNF and tannin molecules. c) The templated nanofibers are then thawed in ethanol solutions rich in metal ions for the formation of the metal–phenolic networks (MPNs) while solvent exchanging water for ethanol. d) The assembly of MPN e) on the templated tannin–CNF facilitates drying under ambient conditions while significantly preventing shrinkage.

of cellulose[36–38] or by cross-linking.[39–41] We further discuss the assembly of MPN in the presence of CNF and investigate the effect of tannin type and concentration on the formation and physicochemical properties of MPN foams, as well as the effect of the type of metal ion used (Figure 1e). A general method to fabricate MPN foams is proposed as a toolbox for the development of functions using all plant-based materials as building blocks.

2. Results and Discussion

The ligand size, its molecular distribution, and its binding capacity toward multivalent metal ions are fundamentally important to develop strong MPN structures.[1,42] Herein, we combined tannin and CNF by cogrinding, resulting in a homogeneous adsorption of the polyphenol on the fibrils.[31,32] We used tannic acid (TA) and condensed tannins (CTs), which share similar origins but feature remarkable differences in terms of phenolic content, functional groups, molecular weight, and 3D molecular arrangement.[43] The resulting modified nanofibers were then used to produce solid MPN foams, as discussed next.

We first investigated the tannin–cellulose interactions and MPN assembly in aqueous suspension. We used iron nitrate for the assembly of the MPNs given its solubility in ethanol, which was later used as a thawing solvent to produce the foams. While tannic acid (**Figure 2**a) is expected to bind more strongly to cellulose compared to the condensed counterpart (CT binding groups are partially sterically hindered) (Figure 2d), the latter are more widely available and are more cost-effective.[44] The UV spectrum of TA-containing nanocellulose (CNF/TA) shows a clear blueshift of the peak assigned to TA (from 275 to 260 nm, Figure 2b,c). The position of the UV-Vis peak remained constant for the CT and CNF/CT systems (Figure 2e,f and Figure S1 (Supporting Information)). CNF/TA and CNF/CT suspensions showed a higher nonspecific absorbance compared to pure TA and CT solutions; however, TA displays a much higher binding capacity with cellulose, which is driven mostly by secondary interactions, mainly hydrogen bonding, van der Waals forces, and CH-π interactions. Both TA and CT are deeply incorporated within the CNF bundles, as indicated by UV–vis peak observed after extensive dialysis of the CNF/tannin suspension (Figure S2, Supporting Information). The tannins exist within the CNF bundles in two different configurations, as an adsorbed layer on cellulose and as free molecules. The latter partially leach out during dialysis, to an extent that depends on the total polyphenols content: a higher tannin content leads to higher leaching. For both tannins, the addition of metal ions leads to MPN assembly regardless the presence or absence of CNF, with an overall broader band for MPN assembled in the presence of CNF (UV–vis spectra of CNF and iron nitrate solution, Figure S3, Supporting Information). This is speculated to be, at least in part, due to molecular conformation caused by the confinement of the assembly in the presence of cellulose fibrils. The less visible changes observed for the CNF/CT system point to a lower binding of CT with the metal ion; however, the MPN is clearly formed as it is also observed by the color change of the suspension – a typical sign of the formation of iron tannates of characteristic purple color (inset Figure 2c,f).

The incorporation of both TA and CT in CNF, at only 10% mass fraction, modified remarkably the rheological properties of the suspension. The presence of tannins increased the apparent viscosity of the CNF suspensions (fibril content of 0.85 wt%) and accentuated their shear thinning behavior (Figure S4, Supporting Information). The subsequent MPN assembly on the tannin-containing CNF surface imparted minor changes in the shear thinning behavior. The storage (G') and loss (G'') moduli of the CNF/tannin and CNF/MPN hydrogels were one order of magnitude higher than those for neat CNF suspension (Figure 2g,h), with the most significant changes occurring in the presence of tannins. Nonetheless, all the suspensions were in a predominantly elastic regime, $G' > G''$ across the 0.1–100 rad s^{-1} angular frequency scan. However, G'' increases at ≈3 rad s^{-1} for pure CNF, while it remained constant until ≈80 rad s^{-1} for the CNF/tannin and CNF/MPN samples. The viscoelastic properties and flow behavior indicate that (at the used CNF concentration: 0.85 wt%) the addition of TA or CT cross-links the CNF network via secondary interactions and to an interlocking of the nanofibrillar network due to the assembly of the MPN. The high viscosity of the CNF/tannins–MPN supramolecular gels, especially measured at low shear rates, impeded direct use as precursors for the fabrication of MPN foams by the traditional FTD method.

We investigated the effect of tannin, as well as MPN formation, on the mechanical properties of a nanocellulose fibril bundle (widths of 20–30 nm) by atomic force microscopy (AFM) operating in force mode (Figure S5a, Supporting Information). Overall, the adsorption and cross-linking effect of tannin on the fibrils increased their flexural stiffness (Figure S5b, Supporting Information). The work of adhesion (and adhesion force, Figure S5c, Supporting Information) was slightly higher for the tannin–CNF compared to the neat CNF, though the networking of the phenol hydroxyls and the $Fe^{(III)}$ ions (MPN formation) decreased their adhesiveness. This is a result of hydrophilic binding sites occupied by the MPN assembly. The CNF/CT system was more adhesive than CNF and CNF/TA, which is due to a heterogenous chemical makeup and larger size resulting in looser binding to cellulose (Figure 2e,f).

The growth of ice crystals among the highly interconnected gel network is not capable of introducing pores and cohesive cell wall structures homogenously across the precursor suspensions. Therefore, the frozen scaffold obtained from both CNF/tannin–MPN precursors collapsed after the thawing–drying (in air) stages, resulting in a foam with volumetric shrinkage of >80% (**Figure 3**a and Figure S6 (Supporting Information)). The shrinkage was extensively reduced (<10%) when assembling the MPN after the tannin–CNFs were already templated, i.e., during the thawing process (Figure 3b,c and Figure S6 (Supporting Information)) and foams with well-defined pores were formed (Figure 3d–g and Figures S7 and S8 (Supporting Information)). CNF suspensions containing 2.5–50 wt% of tannins – TA and CT – relative to the fibril content were ice-templated (at ≈–16 °C) and then thawed in pure ethanol (Figure 3b) and $Fe(NO_3)_3$ ethanol solutions (Figure 3c). We next investigated the effect of $Fe(NO_3)_3$ concentration (0.001–1 g L^{-1}) in the thawing solution over the MPN assembly and shape fidelity after air drying. The shrinkage decreased with metal ion concentration, but no major differences were observed at concentration from

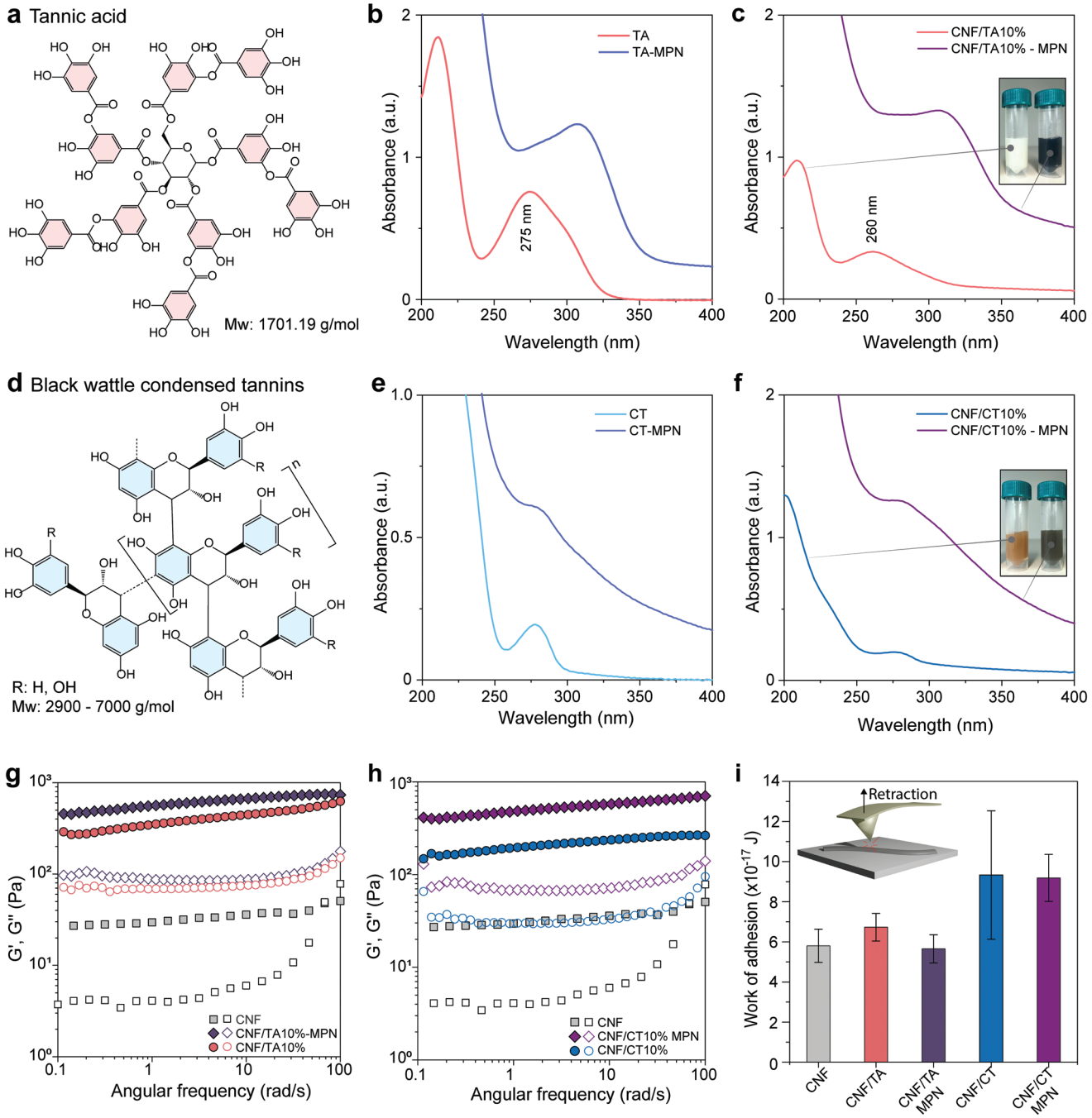

Figure 2. Assembly of the MPN on cellulose nanofibers using a) tannic acid (TA) and d) condensed tannins from black wattle (CT). UV–vis spectra displaying MPN assembly with $Fe^{(III)}$ in the absence b) for TA, e) for CT) and presence of CNF c) for TA, f) for CT). Storage (G', filled symbols) and loss (G'', empty symbols) moduli were obtained via oscillatory rheology of CNF, CNF/tannin, and CNF/tannin–MPN using g) TA and h) CT. i) Work of adhesion (AFM force mode) measured on CNF and modified CNF, as indicated.

0.1 to 1 g L^{-1} (Figure S9, Supporting Information). The resulting foams had densities of 0.015–0.035 g cm^{-3} (Figure S10, Supporting Information), with upper boundaries found in samples containing high tannin contents and thawed in ethanol in the absence of ions.

The tannin–CNF foam resulted in ≈20% shrinkage after thawing–drying (Figure 3a), forming a well-defined pore structure (Figure 3d), characteristic of foam materials.[4] Foams with the lowest density and highest shape fidelity were obtained with 5–10% tannins following thawing in $Fe^{(III)}$–ethanol solutions for MPN assembly (Figure 3e). Thawing the frozen tannin–CNF precursors in pure ethanol sets a tannin limit of 10%, after which the local density of the foam cell walls increases sharply and overcomes the cross-linking capacity of tannins observed at lower mass fractions (Figure 3a), thus leading to 40–60% shrinkage and foam collapse (Figure 3f). Tannins are

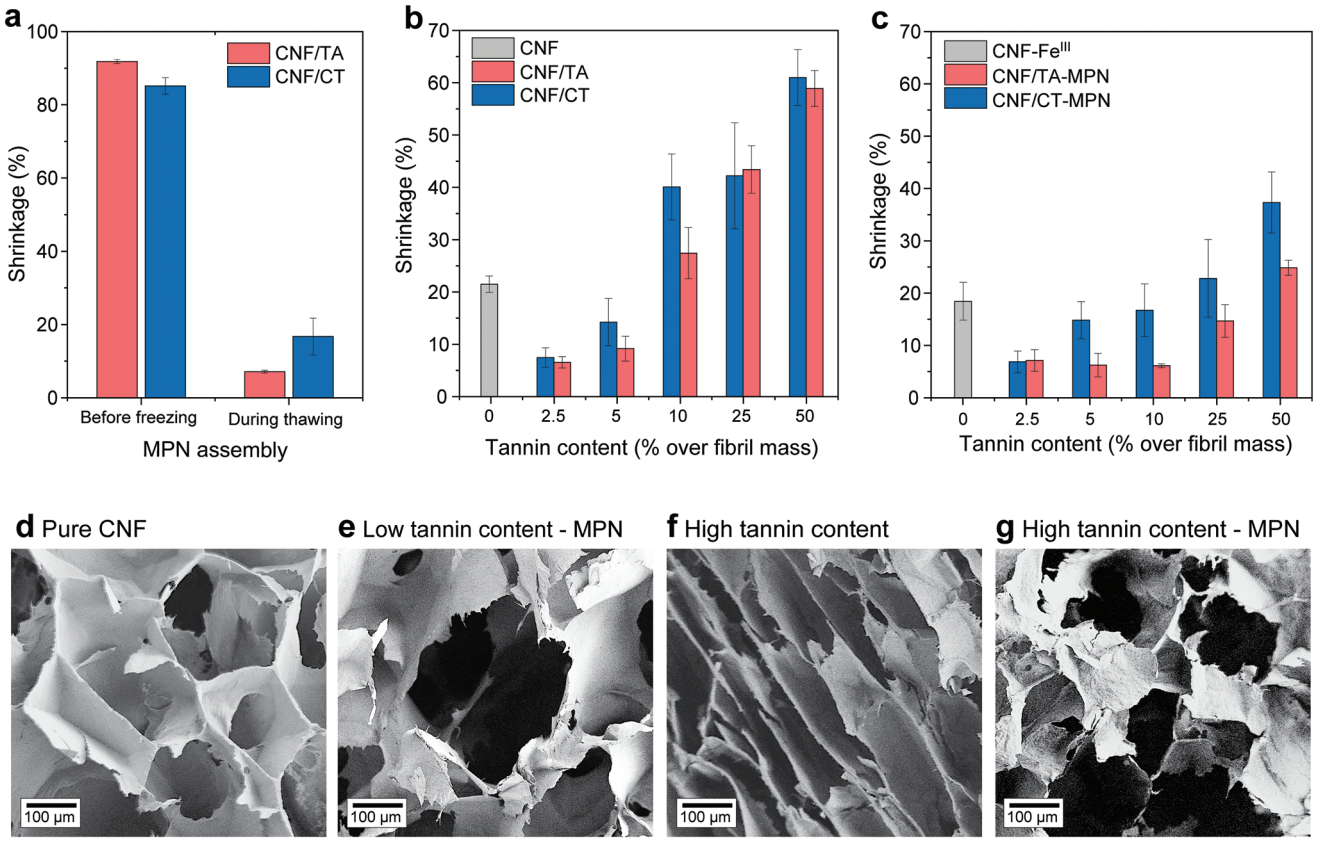

Figure 3. Physical and structural properties of the MPN foams. a) Effect of MPN assembly conditions on the foam shrinkage. b) Shrinkage of CNF/tannin and c) CNF/tannin–MPN foams with increased tannin content. Scanning electron microscopy images of d) pure CNF, e) CNF/TA10%–MPN, f) CNF/TA50%, and g) CNF/TA50%–MPN.

bio-macromolecules that do not form a continuous matrix and are often copolymerized with furfuryl alcohol for material development,[45,46] therefore tannins at a high content (25–50%) within the nanofiber network only act as binders by formation of MPN in the presence of $Fe^{(III)}$. By thawing the tannin–CNF suspensions in $Fe^{(III)}$-rich ethanol, the MPN is formed in situ, and leads to strong cell walls that sustain drying stresses even at tannin contents as high as 50% for the CNF/TA and 25% for CNF/CT systems (Figure 3g). Nevertheless, thawing in ethanol, which coagulates cellulose, is essential to enable high shape fidelity in the resulting MPN foams, as an aqueous $Fe(NO_3)_3$ solution as the thawing medium resulted in 70% shrinkage (Figure S11a, Supporting Information). Moreover, cogrinding tannins with cellulose fibers resulted in strong tannin/cellulose interactions when compared to simple mixing.[31,32] Indeed, coground CNF/tannin led to MPN foams with low volume shrinkage (5–15%) while the mixed systems shrank to a greater extent (15–30%, Figure S11b, Supporting Information).

The MPN foams, with well-organized pore structures (Figure 3e,g), displayed the typical behavior of cellular materials when exposed to uniaxial compressive mechanical stress. The force-strain curves (**Figure 4**a_1,a_2) show the three characteristic stages: i) linear viscoelasticity where the cell walls bend, ii) plateau region due to elastic buckling, and iii) densification regime where the cell walls collapse and make contact.[4] In a collapsed foam (Figure 3f), the first two stages are absent (Figure 4a_1), and the densification stage takes place at very low strains (<5%) when compared to macroporous foams (>40%). We evaluate the strength at 60% strain to compare the various CNF/tannin and MPN foams. Such choice of reference strain is made given that some materials do not present a yield point (i.e., a clear transition between stages i and ii) nor a well-defined elastic regime (stage i). Meanwhile, the strength at 60% can be conveniently compared since all the samples undergo similar mechanical densification regime at this load. Moreover, we normalized the strength by the density (i.e., specific strength), since denser foams inevitably display higher mechanical strength,[4] which would confound the effects of tannin addition and MPN assembly.

By increasing the ion concentration in the thawing solution, stronger MPN foams were formed; however, as noted for the shrinkage, the gains in cohesion plateaued at concentrations from 0.1 to 1 g L^{-1} (Figure S12, Supporting Information). Therefore, we fixed the $Fe(NO_3)_3$ concentration at 1 g L^{-1} and investigated the effect of tannin content and thawing media on the strength of the resulting foams. A remarkable increase (≈40%) in strength was observed in the CNF/tannin foams (i.e., thawed in ethanol) with 2.5–5% of either TA or CT and when compared to pure CNF (Figure 4b_1), thus confirming the ability of plant polyphenols to cross-link the networks by supramolecular interactions.[1] The strength of the CNF/tannin foams was rapidly reduced at a TA/CT content of 10% based on fibril mass,

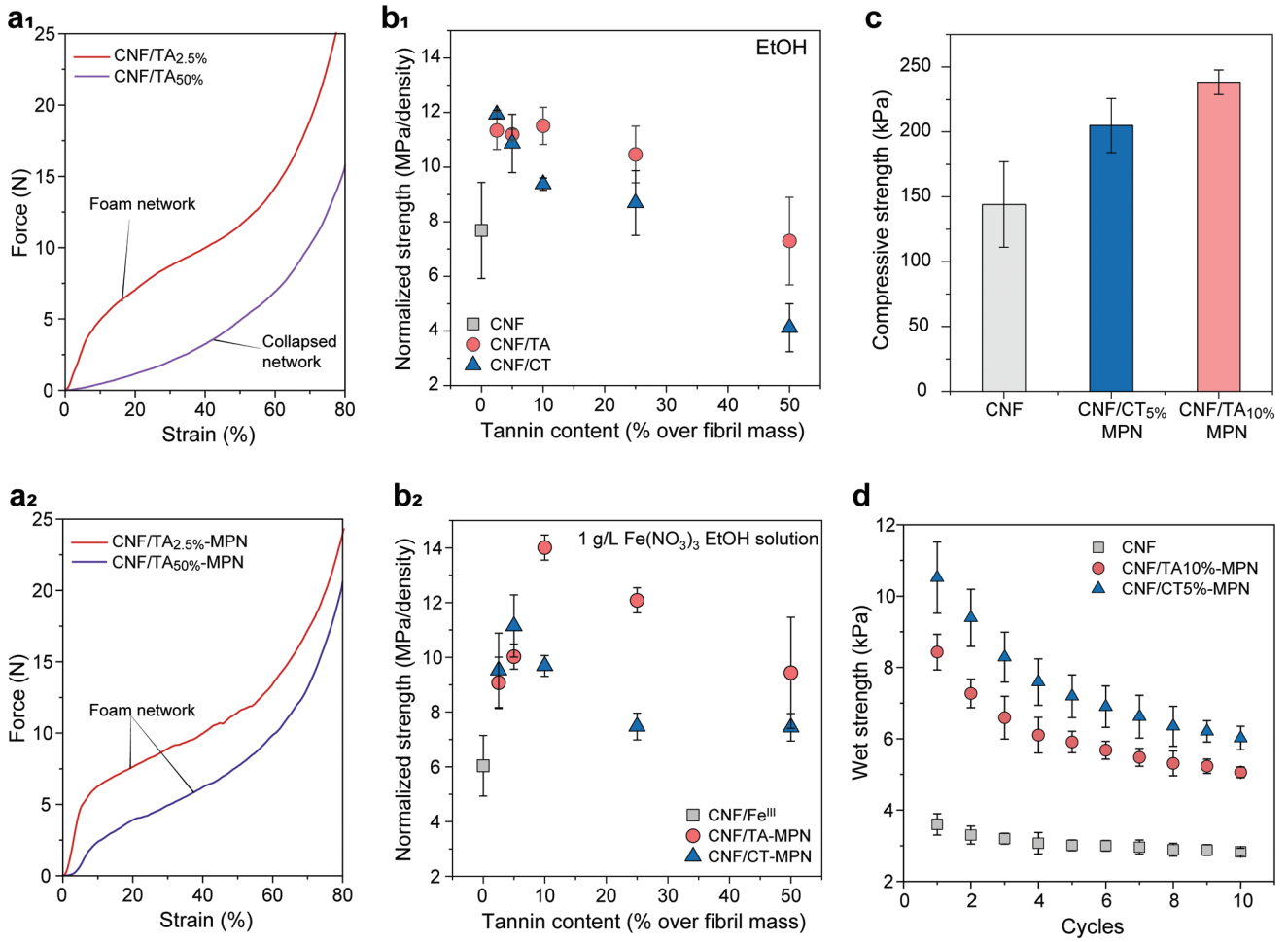

Figure 4. Mechanical performance of MPN foams. a_1,a_2) Effect of the MPN assembly at low and high tannin concentrations on the morphology of the foams and resulting mechanical strength. b) Normalized strength obtained under uniaxial compression stress for CNF/tannin precursors thawed in b_1) pure ethanol and b_2) $Fe(NO_3)_3$ ethanol solution at 1 g L^{-1}. c) Ultimate compressive strength of the MPN foams (optimal conditions) for TA and CT. d) Wet strength of the MPN foams compared to CNF foams under 10 compression cycles.

reaching values lower than those for pure CNF when added at high tannin contents (50%). The increase in the local density across the pore cell walls, and the extensive content of loosely bound tannins overcame their cross-linking ability, resulting in poorer mechanical properties.

As far as cohesion development in the MPN foams, a narrow window of tannin content maximized the strength, depending on the type of tannin used. The strength peaked at 10% and 5% tannin for MPN foams assembled with TA and CT, respectively (Figure 4b_2). In each case, higher tannin addition led to a weaker system, but to a lesser extent when compared to the CNF/tannin foams – without MPN assembly. We speculate that the specific strength of CT–MPN foams (Figure 4b_2) peaked at lower contents compared to the TA analog because of macromolecular configuration. The larger dimensions of CNF exposed to the low-molecular weight TA compared to CT molecules (Figure 2a,d) imparts a premature surface saturation by the latter, thus limiting cross-linking.

At optimized conditions (5% CT or 10% TA), MPN foams presented a compressive strength of ≈250 kPa, ≈70% stronger than those from neat CNF (Figure 4c). Most importantly, the assembly of MPN is shown as an effective way of introducing metal ions into the porous materials, without disrupting the cellulose–cellulose interactions, which are key to developing cohesion. This can be observed by comparing the strength of CNF foams when thawed in $Fe^{(III)}$-free and $Fe^{(III)}$-containing ethanol: a 25% reduction is observed when CNF foams are consolidated in the presence of metal ions due to the disruption of cellulose O—H···O interactions by (longer-range) $Fe^{+}\cdots O^{-}$ (cellulose) electrostatic interactions. Nevertheless, the MPN formed with the fibrils yielded foams with high resilience and shape recovery properties, as noted after compression cycles under a strain that was increased gradually up to 60% (Figure S13, Supporting Information). In addition, a higher wet strength was noted when compared to pure CNF foams (Figure 4d). The compressive strength was recorded at 30% strain (a point at which cell walls are bending but still in the range where all samples recover their initial shape, Figure S13, Supporting Information) over 10 cycles in foams wetted immediately before the tests (Figure 4d and Figure S14 (Supporting Information)). We observe that the MPN foams not only were less hydrophilic (visual wetting), but that after 10 cycles, the wet

strength of MPN foams was twice than that of CNF foams. Due to its condensed structure, and low exposure of hydrophilic groups, CT–MPN foams were more water-resistant, confirming conclusions obtained with hydrophobic CT–CNF films.[31]

Among other applications, MPNs enabled by $Fe^{(III)}$ have been shown to display high fire resistance;[47] however, CNFs (and cellulose in general) are highly flammable. Therefore, as a demonstration of the attributes of the $Fe^{(III)}$ CNF–MPN foams, and the ability of MPNs to endow CNF porous matrices with new functions, we evaluated their fire resistance taking into consideration tannin type and content (Figure S15a,b, Supporting Information). Neat CNF, tannin–CNF, and MPN–CNF foams were exposed to a butane flame and their mass loss was recorded for 2 min. As expected, complete combustion occurred rapidly (in ≈30 s) when CNF foams were directly exposed to the butane flame. Comparatively, the tannin–CNF foams displayed flame resistance, especially when 25% of tannin was used. In this latter case, the condensed tannin structures led to high char content, resulting in a residual mass of ≈40% after 2 min exposure. The results of flame resistance are in line with reports on the effect brought by the tannins when added to fire-sensitive precursors.[48,49] After addition of the $Fe^{(III)}$ ions, for MPN assembly, the fire resistance of the resulting foams increased significantly, including those prepared at tannin concentrations as low as 5%. In this case, the mass loss is limited to ≈25% in the MPN–CNF foams, which is a remarkable improvement when compared to neat CNF foams (Figure S15b, Supporting Information).

So far, $Fe^{(III)}$ ions have been used to demonstrate the method and its property boundaries as far as tannin content and type, as well as application potential. We next describe a general framework to create MPN foams using tannin-containing CNF. However, MPNs can be assembled with a variety of metal ions.[20] In our FTD method, the only limiting factor related to the metal ion is its solubility in ethanol. Therefore, we used EtOH-soluble nitrate salts of yttrium (Y), gallium (Ga), neodymium (Nd), chromium (Cr), cerium (Ce), aluminum (Al), copper (Cu), calcium (Ca), magnesium (Mg), zinc (Zn), and nickel (Ni) to investigate the versatility of the method and to understand the effect of the metal ion on the properties of the resulting MPN foams. Note: we avoided any effect from a different counterion present in the medium during the consolidation of the foams.[50]

We fixed TA and CT content at 10% and observed a clear effect of the metal ion on the resulting mechanical strength of the MPN foams (**Figure 5**a), whereas the shrinkage of the MPN foams was impacted by the metal ion by a lesser extent (Figure S16, Supporting Information). The shrinkage of the $Fe^{(III)}$ CNF/TA–MPN foams was ≈6%, while the other ions resulted in MPN foams with shrinkage values in the range between 6% and 9%. The highest values were observed in MPN foams assembled with bivalent metal cations. Similar observations were made for CNF/CT–MPN foams, albeit they resulted in higher shrinkage levels (≈15–22%). Although the specific compression strength ranged from 5 to 15 MPa $(g\ cm^{-3})^{-1}$, all MPN foams were mechanically robust and displayed high shape fidelity, as observed for $Cu^{(II)}$ CNF/CT–MPN, $Al^{(III)}$ CNF/TA–MPN, $Ce^{(III)}$

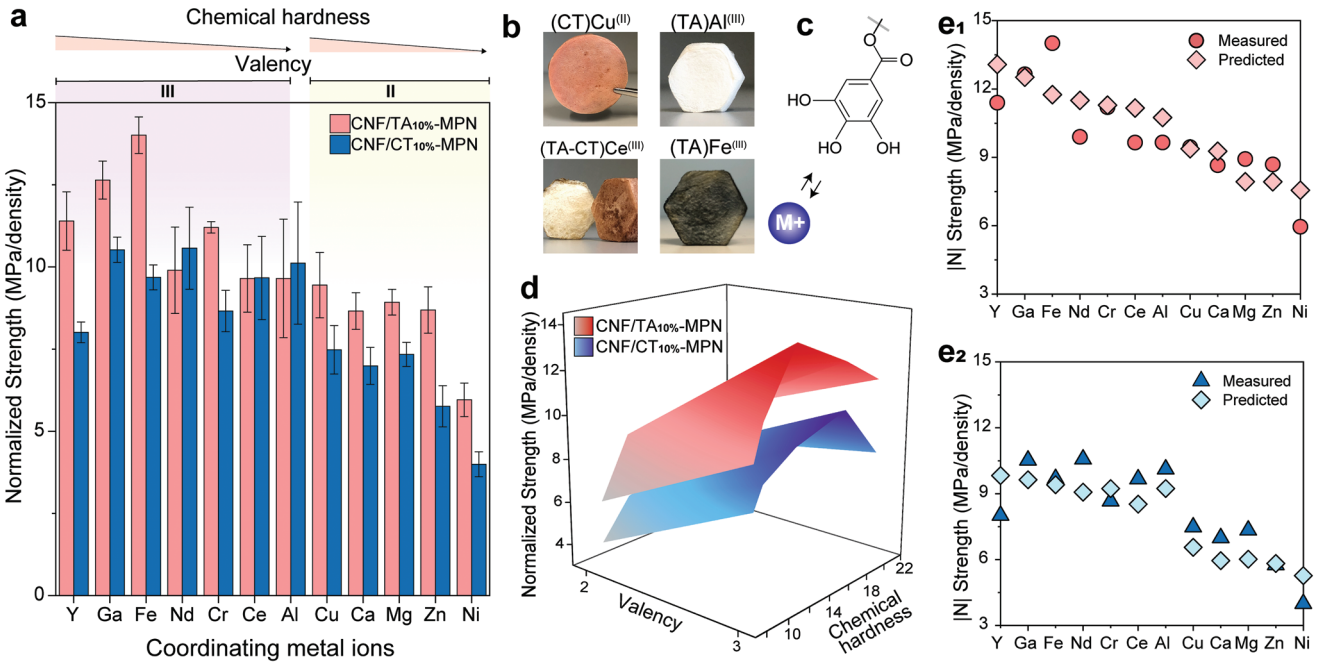

Figure 5. Versatility of the freeze–thawing–drying (FTD) method to fabricate MPN foams. a) Normalized strength of MPN foams prepared at TA and condensed tannin (CT) contents fixed at 10%, but with various metal ions. b) Visual examples of MPN foams obtained with the FTD method, including $Cu^{(II)}$ CNF/CT–MPN, $Al^{(III)}$ CNF/TA–MPN, $Ce^{(III)}$ CNF/TA–MPN and $Ce^{(III)}$ CNF/CT–MPN, and $Fe^{(III)}$ CNF/TA–MPN. c) The cohesion of the MPN network and, consequently, the foam depends on the ligand–metal binding, which was assessed using d) 3D map of specific strength as a function of valency and chemical hardness. e) MLR model, accounting for valency and chemical hardness, can predict with high accuracy the cohesion of the e_1) CNF/TA- and e_2) CNF/CT-based MPN foams.

CNF/TA–MPN, and $Ce^{(III)}$ CNF/CT–MPN, as well as the $Fe^{(III)}$ CNF/TA–MPN (Figure 5b). The only factor varying was the ion–ligand interaction taking place during the MPN assembly (Figure 5c). We used multiple linear regression (MLR) to empirically assess the relevance of the properties of the chosen metal ion on the metal–tannin interactions that lead to MPN formation and affected the mechanical properties of the produced foams (Figure 5d). We used the valency and the chemical hardness of the metal ion to fit the results via MLR. The lack of correlation in the MLR partials (Figure S17, Supporting Information) indicates that none of the chosen ion properties individually explain the resulting cohesion of the MPN; however, valency has a more important effect than the second most relevant property, i.e., chemical hardness (Figure S18, Supporting Information). The charge of the respective metal ion, i.e., its valency, has been reported to play a key role in the MPN formation,[51] since multivalent ions form covalent cross-links with polyphenols.[52] The higher the valency, the more binding sites are available and higher cross-linking density can be achieved, explaining the strong influence on the foam properties. Apart from valency, we used the chemical hardness, a numerical value calculated based on the "hard and soft acids and bases" (HSAB) concept, also known as the Pearson acid base concept.[53] The HSAB was used to explain the stability of bonds, in which, compared to a soft specie, a hard specie has a small radius, a high charge density, and is less polarizable.[53] Based on the HSAB concept, a hard acid and a hard base form a stronger bond than a combination of hard and soft, and vice versa. The chemical hardness considers the electronic energy and is proportional to the ionization potential and electron affinity,[53] which can differ significantly also in between metals with the same valency and are dependent on the electron configuration of the ion.

When plotting a 3D map of the strength as a function of valency and chemical hardness, we observed a performance that is consistent across tannin ligands. The strength of the MPN foams was maximized when using metal ions of valency 3 and hardness ranging from 12 to 16 eV (Figure 5d). This range is noted to be the best match of hard–hard interactions between the metallic ions and the OH^- (a hard basis with hardness of 6.8 eV) from the ligand in the assembly of cohesive metal–phenolic networks. MLR models built with the original data were prepared to determine the strength by using valency and chemical hardness as independent variables. Figure $5e_1,e_2$ shows that valency and hardness of the metal ions predict with good accuracy the strength of the resulting MPN foams. There are certain outliers in the model, which are likely due to the rather complex MPN network formed and other effects such as local pH environment.[54,55] Moreover, our empirical MLR model is demonstrated to be a straightforward tool to support further optimization of properties of CNF-enabled MPN porous materials, as well as several other MPN nanostructures (e.g., capsules and films).

3. Conclusions

We developed a robust and versatile framework to fabricate MPN foams, whose physical–mechanical properties are tailorable by selecting the type and concentration of polyphenolic ligands, i.e., tannic acid or condensed tannin. The method consists of promoting the assembly of MPNs in situ after the tannin-containing CNFs have been already ice-templated. With this strategy, one can obtain foams with compression strengths as high as 250 kPa, and shrinkage as low as ≈5%. The content and type of tannin can be easily manipulated to tailor the foam structure and density of metal ions. Due to the varying tested metal–ligand interactions, a toolbox for preparing MPN foams with predictable properties is possible. CNF/condensed-tannin-based MPN foams were weaker, due to the lower ability of condensed polyphenol to bind multivalent metal ions. Overall, this work describes a freezing–thawing–drying method to fabricate MPN foams and factors the influence of tannin type, content, and metal ion used for MPN assembly. The resulting foams can be further applied in, for example, catalytic platforms based on Fenton reactions in $Fe^{(III)}$-based MPN,[21] batteries for $Zn^{(II)}$-based MPN,[56] fire-retardant materials (Figure S15, Supporting Information) and coatings,[47] and antimicrobial materials for $Cu^{(II)}$-based MPN,[57] among others. However, more studies are required to assess the stability of MPN foams in technically relevant media, for instance, for given solvents and electrolytes.

4. Experimental Section

Materials: Iron(III) nitrate nonahydrate (CAS no. 7782-61-8), nickel(II) nitrate hexahydrate (13478-00-7), neodymium(III) nitrate hexahydrate (16454-60-7), copper(II) nitrate trihydrate (10031-43-3), aluminum(III) nitrate nonahydrate (7784-272), zinc nitrate hexahydrate (10196-18-6), cerium(III) nitrate hexahydrate (10294-41-4), calcium nitrate tetrahydrate (13477-34-4), gallium(III) nitrate hydrate (69365-72-6), yttrium(III) nitrate hexahydrate (13494-98-9), chromium(III) nitrate nonahydrate (7789-02-8), and magnesium nitrate hexahydrate (13446-18-9) were purchased from Merck and used as received. Two tannin types were considered, TA (1401-55-4) supplied by Merck, and a CT extracted from the bark of black wattle (*Acacia mearnsii*), which was kindly donated by TANAC S/A Brazil. Ethanol (99.5% purity) was purchased from Anora Industrial Oyj, Finland.

Preparation of Tannin-Containing CNF: Never-dried bleached kraft birch pulp was diluted to 0.85% w/v in deionized water. TA or CT was added to the fiber suspension (2.5%, 5%, 10%, 25%, and 50% over mass of fibers) under gentle agitation. The fibers were first processed in a high-shear homogenizer for 5 min at 10 000 RPM (T18 ULTRA-TURRAX – IKA) and then fibrillated using a high-pressure microfluidizer (Microfluidics M110P) operating with one pass through 400–200 µm chamber followed with 6 passes in a 200–100 µm chamber at 2000 bar.

MPN Foam: CNF suspensions, containing or not tannins, were cast in 5 mL polydimethylsiloxane containers and immediately placed in a freezer at –16 °C where they were kept for 12 h. The frozen precursors were thawed for 2 h in either pure ethanol or ethanol solutions containing metal nitrates at given concentrations. Then, the samples thawed in metal solutions were transferred to pure ethanol for another 2 h, in order to remove any excess or unbound metal ions. A volume ratio of 20:1 of thawing/washing medium to frozen suspension was used for all samples. The samples were removed from the container and allowed to dry in air at room temperature (25 °C) until reaching constant mass, and then they were placed in an oven at 60 °C for 1 h to eliminate residual ethanol. The dimensions of the frozen system and dried foams were used to calculate the shrinkage after drying.

Mechanical Characterization: The mechanical strength of the foams was evaluated by uniaxial compression using a TA.XTplusC Texture Analyzer. The measurements were carried out at a compression rate of 0.10 mm s^{-1} and within a conditioned environment (23 °C and 50% of relative humidity).

UV–Vis: The UV–vis absorbance of the CNF, tannins, iron nitrate solutions, and their combinations was recorded in a Shimadzu UV-2550 spectrophotometer (Shimadzu Corporation, Kyoto, Japan) in the wavelength range of 200–800 nm. All measurements were carried out at room temperature.

Rheology: The apparent viscosity was measured using a rheometer (MCR 302, Anton Paar, Germany) equipped with parallel plates (PP25) and a gap fixed at 1 mm. The shear viscosity was monitored at varying shear rates (0.01–100 s^{-1}). For dynamic viscoelastic measurements, the linear viscoelastic range was determined with a strain sweep (0.01–100%) at a fixed frequency of 10 rad s^{-1}. After this, a dynamic frequency sweep (0.1 and 100 rad s^{-1}) was conducted using the parallel plate geometry (PP25) with a gap fixed at 1 mm and by applying a constant strain of 0.1%, which was within the nearly linear region. The dynamic profiles were obtained by recording the storage (G') and loss (G'') moduli as function of frequency. All measurements were performed at 23 °C. The use of a covered parallel plate edge was noted by using silica oil, which prevented sample evaporation during the tests.

Imaging by Scanning Electron Microscopy (SEM): Field-emission SEM was carried out in a Zeiss Sigma (VP, Germany) using an acceleration voltage of 1.5 kV. The samples were coated with a 4 nm thick gold/palladium layer on a Leica EM ACE600 high vacuum sputter coater.

Indentation/Adhesion by Atomic Force Microscopy: CNF, CNF/tannins, and CNF/tannins–MPN suspensions were diluted to 0.01 mg L^{-1} (over fibril mass) and then dip cast on a freshly cleaved mica substrate. The samples were allowed to air dry before indentation/adhesion experiments. The force curves were obtained in a Nanowizard 4 (Bruker, Germany) AFM using a cantilever with an 8 nm radius spherical tip (nominal spring constant of 40 N m^{-1} and a resonance frequency of ≈260 kHz). QI mode was used to obtain force–distance curves in several places on 20–30 nm wide fibril bundles. The vertical deflection was set at 200 nN, with 100 nm approach and retract distances at a 2 µm s^{-1} rate.

Fire Retardancy Assay: The resistance of the MPN foams to fire was assessed using a butane flame (burning temperature of ≈1500 °C) in contact with the samples for 2 min. The mass loss was used as a quantitative result of the fire retardancy of the foams, further verified by photographs taken during the burning tests.

Statistical Analysis: Descriptive statistical analysis was used to describe the data obtained in the experiments related to the physical and mechanical properties. The normal distribution of the data was verified before plotting the averaged result along with its standard deviation. MLR was used to identify the most important factors, related to the metal ions affecting the strength of MPN foams. For this, nontransformed data of strength were used as dependent variable, and valency and chemical hardness as independent variables. The quality of the fitting was verified by the residual sum of squares, coefficient of determination, and value P. The weight of each variable on the resulting property was assessed using the values of the MLR coefficients corresponding to each independent variable. At least five replicates were used in each (quantitative) experiment.

Supporting Information

Supporting Information is available from the Wiley Online Library or from the author.

Acknowledgements

The authors acknowledge funding support from the European Research Council (ERC) under the European Union's Horizon 2020 research and innovation program (Grant Agreement No. 788489, "BioElCell"); the Canada Excellence Research Chair Program (Grant No. CERC-2018-00006); the FAPERGS (Research Support Foundation of the State of RS), Process Number: 21/2551-0000603-0; the Canada Foundation for Innovation (Project No. 38623); and the São Paulo Research Foundation (FAPESP, Grant No. 2021/12071-6). The authors also appreciate the support of the Academy of Finland Bioeconomy Flagship, FinnCERES Materials Cluster.

Conflict of Interest

The authors declare no conflict of interest.

Data Availability Statement

The data that support the findings of this study are available from the corresponding author upon reasonable request.

Keywords

cellulose nanofibers, in situ freeze–thawing–drying, metal–phenolic coordination, solid foams

Received: October 20, 2022
Revised: January 31, 2023
Published online: February 12, 2023

[1] B. L. Tardy, B. D. Mattos, C. G. Otoni, M. Beaumont, J. Majoinen, T. Kämäräinen, O. J. Rojas, *Chem. Rev.* **2021**, *121*, 14088.
[2] N. Mittal, F. Ansari, V. K. Gowda, C. Brouzet, P. Chen, P. T. Larsson, S. V. Roth, F. Lundell, L. Wågberg, N. A. Kotov, L. D. Söderberg, *ACS Nano* **2018**, *12*, 6378.
[3] Z. Hongli, Z. Shuze, J. Zheng, P. Sepideh, L. Yuanyuan, V. Oeyvind, H. Liangbing, L. Teng, *Proc. Natl. Acad. Sci. USA* **2015**, *112*, 8971.
[4] N. Lavoine, L. Bergström, *J. Mater. Chem. A* **2017**, *5*, 16105.
[5] R. Abidnejad, M. Beaumont, B. L. Tardy, B. D. Mattos, O. J. Rojas, *ACS Nano* **2021**, *15*, 19712.
[6] B. Wicklein, A. Kocjan, G. Salazar-Alvarez, F. Carosio, G. Camino, M. Antonietti, L. Bergström, *Nat. Nanotechnol.* **2015**, *10*, 277.
[7] K. B. R. Teodoro, R. C. Sanfelice, F. L. Migliorini, A. Pavinatto, M. H. M. Facure, D. S. Correa, *ACS Sens.* **2021**, *6*, 2473.
[8] Q. Wang, R. Zhou, J. Sun, J. Liu, Q. Zhu, *ACS Nano* **2022**, *16*, 13468.
[9] M. Beaumont, P. Jusner, N. Gierlinger, A. W. T. King, A. Potthast, O. J. Rojas, T. Rosenau, *Nat. Commun.* **2021**, *12*, 2513.
[10] E. Ahn, T. Kim, Y. Jeon, B.-S. Kim, *ACS Nano* **2020**, *14*, 6173.
[11] S. Hu, Y. Zhi, S. Shan, Y. Ni, *Carbohydr. Polym.* **2022**, *275*, 118741.
[12] X. Fan, Y. Guan, Y. Li, H.-Y. Yu, J. Marek, D. Wang, J. Militky, Z.-Y. Zou, J. Yao, *ACS Appl. Nano Mater.* **2020**, *3*, 1741.
[13] R. T. Olsson, M. A. S. Azizi Samir, G. Salazar-Alvarez, L. Belova, V. Ström, L. A. Berglund, O. Ikkala, J. Nogués, U. W. Gedde, *Nat. Nanotechnol.* **2010**, *5*, 584.
[14] S.-C. Li, B.-C. Hu, L.-M. Shang, T. Ma, C. Li, H.-W. Liang, S.-H. Yu, *Adv. Mater.* **2022**, *34*, 2202504.
[15] E. Pasquier, B. D. Mattos, N. Belgacem, J. Bras, O. J. Rojas, *Biomacromolecules* **2021**, *22*, 880.
[16] A. Wang, J. Li, T. Zhang, *Nat. Rev. Chem.* **2018**, *2*, 65.
[17] X. Ma, H. Liu, W. Yang, G. Mao, L. Zheng, H.-L. Jiang, *J. Am. Chem. Soc.* **2021**, *143*, 12220.
[18] H. Zhu, X. Yang, E. D. Cranston, S. Zhu, *Adv. Mater.* **2016**, *28*, 7652.
[19] G. Fan, J. Cottet, M. R. Rodriguez-Otero, P. Wasuwanich, A. L. Furst, *ACS Appl. Bio Mater.* **2022**, *5*, 4687.
[20] J. Guo, Y. Ping, H. Ejima, K. Alt, M. Meissner, J. J. Richardson, Y. Yan, K. Peter, D. von Elverfeldt, C. E. Hagemeyer, F. Caruso, *Angew. Chem., Int. Ed.* **2014**, *53*, 5546.

[21] B. L. Tardy, J. J. Richardson, J. Guo, J. Lehtonen, M. Ago, O. J. Rojas, *Green Chem.* **2018**, *20*, 1335.
[22] H. Geng, Q.-Z. Zhong, J. Li, Z. Lin, J. Cui, F. Caruso, J. Hao, *Chem. Rev.* **2022**, *122*, 11432.
[23] M. A. Rahim, M. Björnmalm, T. Suma, M. Faria, Y. Ju, K. Kempe, M. Müllner, H. Ejima, A. D. Stickland, F. Caruso, *Angew. Chem., Int. Ed.* **2016**, *55*, 13803.
[24] M. V. Limaye, C. Schütz, K. Kriechbaum, J. Wohlert, Z. Bacsik, M. Wohlert, W. Xia, M. Pléa, C. Dembele, G. Salazar-Alvarez, L. Bergström, *Nanoscale* **2019**, *11*, 19278.
[25] J. Chen, J. Li, J. Zhou, Z. Lin, F. Cavalieri, E. Czuba-Wojnilowicz, Y. Hu, A. Glab, Y. Ju, J. J. Richardson, F. Caruso, *ACS Nano* **2019**, *13*, 11653.
[26] J. Guo, B. L. Tardy, A. J. Christofferson, Y. Dai, J. J. Richardson, W. Zhu, M. Hu, Y. Ju, J. Cui, R. R. Dagastine, I. Yarovsky, F. Caruso, *Nat. Nanotechnol.* **2016**, *11*, 1105.
[27] Q.-Z. Zhong, J. J. Richardson, S. Li, W. Zhang, Y. Ju, J. Li, S. Pan, J. Chen, F. Caruso, *Angew. Chem., Int. Ed.* **2020**, *59*, 1711.
[28] Y. Qin, J. Wang, C. Qiu, Y. Hu, X. Xu, Z. Jin, *ACS Sustainable Chem. Eng.* **2019**, *7*, 17379.
[29] Q. Dai, Q. Yu, Y. Tian, X. Xie, A. Song, F. Caruso, J. Hao, J. Cui, *ACS Appl. Mater. Interfaces* **2019**, *11*, 29305.
[30] A. L. Missio, B. Tischer, P. S. B. dos Santos, C. Codevilla, C. R. de Menezes, J. S. Barin, C. R. Haselein, J. Labidi, D. A. Gatto, A. Petutschnigg, G. Tondi, *Sep. Purif. Technol.* **2017**, *186*, 218.
[31] A. L. Missio, B. D. Mattos, D. de F Ferreira, W. L. E. Magalhães, D. A. Bertuol, D. A. Gatto, A. Petutschnigg, G. Tondi, *J. Cleaner Prod.* **2018**, *184*, 143.
[32] A. L. Missio, B. D. Mattos, C. G. Otoni, M. Gentil, R. Coldebella, A. Khakalo, D. A. Gatto, O. J. Rojas, *Biomacromolecules* **2020**, *21*, 1865.
[33] T. L. Church, K. Kriechbaum, C. Schiele, V. Apostolopoulou-Kalkavoura, S. E. Hadi, L. Bergström, *Biomacromolecules* **2022**, *23*, 2595.
[34] K. Kriechbaum, V. Apostolopoulou-Kalkavoura, P. Munier, L. Bergström, *ACS Sustainable Chem. Eng.* **2020**, *8*, 17408.
[35] C. Antonini, T. Wu, T. Zimmermann, A. Kherbeche, M.-J. Thoraval, G. Nyström, T. Geiger, *Nanomaterials* **2019**, *9*, 1142.
[36] S. Ma, C. Liu, Y. Xu, L. Wang, H. Wang, W. Xu, Y. Zhuang, H. Yang, *J. Phys. Chem. B* **2021**, *125*, 5853.
[37] R. Gavillon, T. Budtova, *Biomacromolecules* **2008**, *9*, 269.
[38] T. Budtova, *Cellulose* **2019**, *26*, 81.
[39] A. S. González-Ugarte, I. Hafez, M. Tajvidi, *Sci. Rep.* **2020**, *10*, 17459.
[40] H. Fang, N. Feng, D. Wu, D. Hu, *Biomacromolecules* **2021**, *22*, 4155.
[41] L. Liu, L. Bai, A. Tripathi, J. Yu, Z. Wang, M. Borghei, Y. Fan, O. J. Rojas, *ACS Nano* **2019**, *13*, 2927.
[42] W. Xie, Z. Guo, L. Zhao, Y. Wei, *Theranostics* **2021**, *11*, 6407.
[43] D. E. García, W. G. Glasser, A. Pizzi, S. P. Paczkowski, M.-P. Laborie, *New J. Chem.* **2016**, *40*, 36.
[44] P. V. Dhawale, S. K. Vineeth, R. V. Gadhave, J. Fatima M J, M. V. Supekar, V. K. Thakur, P. Raghavan, *Mater. Adv.* **2022**, *3*, 3365.
[45] A. L. Missio, C. G. Otoni, B. Zhao, M. Beaumont, A. Khakalo, T. Kämäräinen, S. H. F. Silva, B. D. Mattos, O. J. Rojas, *ACS Sustainable Chem. Eng.* **2022**, *10*, 10303.
[46] C. Lacoste, M. C. Basso, A. Pizzi, M.-P. Laborie, A. Celzard, V. Fierro, *Ind. Crops Prod.* **2013**, *43*, 245.
[47] Z. Yang, W. Guo, P. Yang, J. Hu, G. Duan, X. Liu, Z. Gu, Y. Li, *Polymer* **2021**, *221*, 123627.
[48] S. Nam, B. D. Condon, Z. Xia, R. Nagarajan, D. J. Hinchliffe, C. A. Madison, *J. Anal. Appl. Pyrolysis* **2017**, *126*, 239.
[49] Y.-O. Kim, J. Cho, H. Yeo, B. W. Lee, B. J. Moon, Y.-M. Ha, Y. R. Jo, Y. C. Jung, *ACS Sustainable Chem. Eng.* **2019**, *7*, 3858.
[50] S.-A. Jin, E. G. Facchine, S. A. Khan, O. J. Rojas, R. J. Spontak, *J. Colloid Interface Sci.* **2021**, *599*, 207.
[51] P. Wasuwanich, G. Fan, B. Burke, A. L. Furst, *J. Mater. Chem. B* **2022**, *10*, 7600.
[52] Z. Zhang, L. Xie, Y. Ju, Y. Dai, *Small* **2021**, *17*, 2100314.
[53] R. G. Pearson, *J. Am. Chem. Soc.* **1988**, *110*, 7684.
[54] T. Benselfelt, M. Nordenström, S. B. Lindström, L. Wågberg, *Adv. Mater. Interfaces* **2019**, *6*, 1900333.
[55] N. Mittal, T. Benselfelt, F. Ansari, K. Gordeyeva, S. V. Roth, L. Wågberg, L. D. Söderberg, *Angew. Chem., Int. Ed.* **2019**, *58*, 18562.
[56] M. Iturrondobeitia, O. Akizu-Gardoki, O. Amondarain, R. Minguez, E. Lizundia, *Adv. Sustainable Syst.* **2022**, *6*, 2100308.
[57] X. Li, P. Gao, J. Tan, K. Xiong, M. F. Maitz, C. Pan, H. Wu, Y. Chen, Z. Yang, N. Huang, *ACS Appl. Mater. Interfaces* **2018**, *10*, 40844.